Supporting Information

Elucidating the Active Sites for CO_2 Electroreduction on Ligand-protected Au_{25} Nanoclusters

Natalie Austin[a], Shuo Zhao[b], James R. McKone[a], Rongchao Jin[b] and Giannis Mpourmpakis[a,*]

a. Department of Chemical Engineering, University of Pittsburgh, Pittsburgh, PA 15261, USA
b. Department of Chemistry, Carnegie Mellon University, Pittsburgh, PA 15213, USA

Table S1. Relative energies (to the lowest energy system) of the Au_{25} nanoclusters optimized with different multiplicities.

	M1	M3	M5
$Au_{25}(SCH_3)_{18}^-$	0	0.96	1.88
$Au_{25}(SCH_3)_{18}^+$	0	0.13	1.15
$Au_{25}(SCH_3)_{17}^0$	0	0.53	1.51
$Au_{25}S(SCH_3)_{17}^0$	0	0.38	1.43
	M2	M4	M6
$Au_{25}(SCH_3)_{18}^0$	0	0.98	1.96
$Au_{25}(SCH_3)_{17}^-$	0	0.93	2.03
$Au_{25}S(SCH_3)_{17}^-$	0	0.95	1.98
$Au_{25}(SCH_3)_{17}^+$	0	0.60	1.80
$Au_{25}S(SCH_3)_{17}^+$	0	0.44	1.60

Table S2. Computed adiabatic electron affinities (AEA) and adiabatic ionization potentials (AIP) of $Au_{25}(SCH_3)_{18}^0$, $Au_{25}(SCH_3)_{17}^0$, and $Au_{25}S(SCH_3)_{17}^0$ in eV

	AEA	**AIP**
$Au_{25}(SCH_3)_{18}^0$	-2.90	5.10
$Au_{25}(SCH_3)_{17}^0$	-2.41	5.20
$Au_{25}S(SCH_3)_{17}^0$	-2.63	5.29

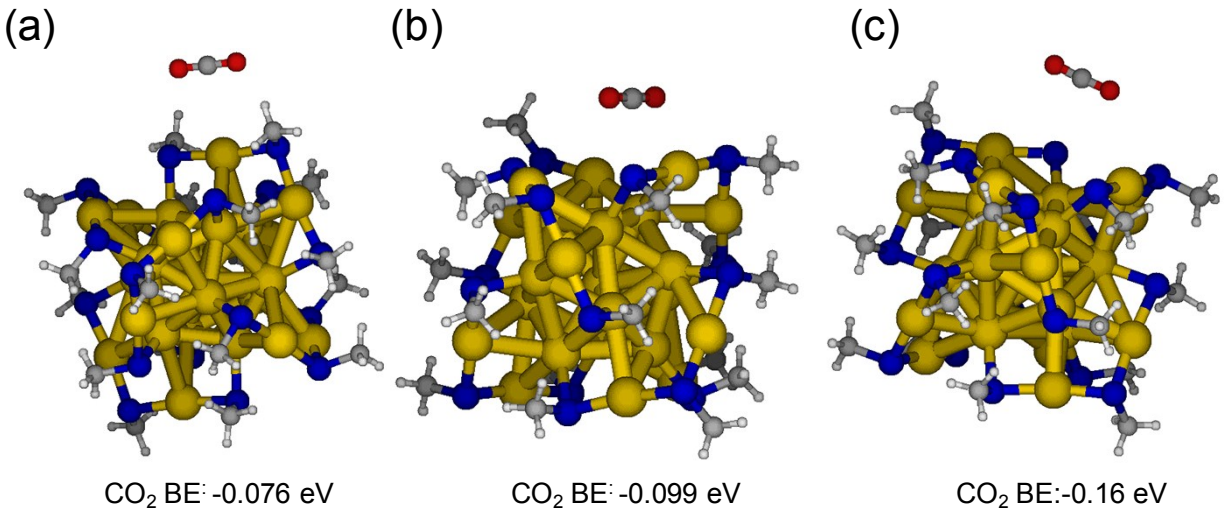

Figure S1. CO_2 adsorption on the negatively charged nanoclusters (a) $Au_{25}(SCH_3)_{18}^-$, (b) $Au_{25}(SCH_3)_{17}^-$, (c) $Au_{25}S(SCH_3)_{17}^-$. Note that physisorption was observed on all the nanoclusters in this study (range: -0.07 to -0.16 eV).

	Site A of removed SCH_3	Site B of removed SCH_3
	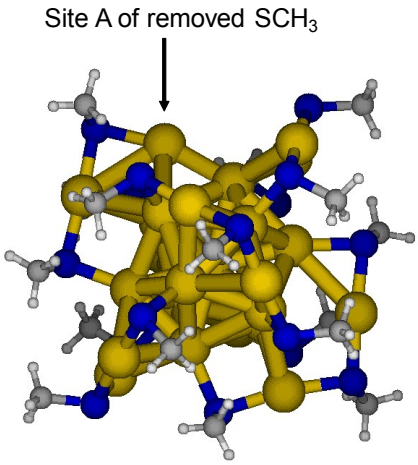	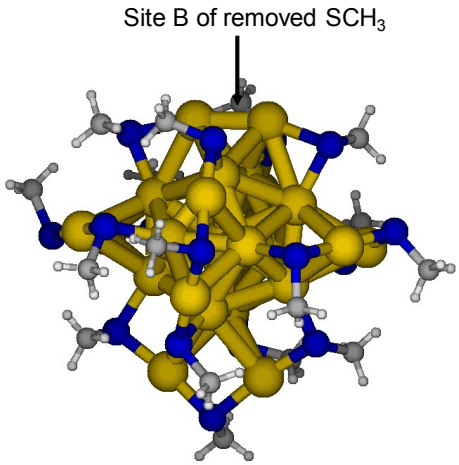
ΔE(-)	1.11	1.37
ΔE(0)	0.65	1.30
ΔE(+)	0.75	1.47

Figure S2. Changes in electronic energy (ΔE) for the reaction step of SCH_3 removal from Site A and Site B (shown in manuscript) of the $Au_{25}(SCH_3)_{18}^-$ NC (values are in eV).

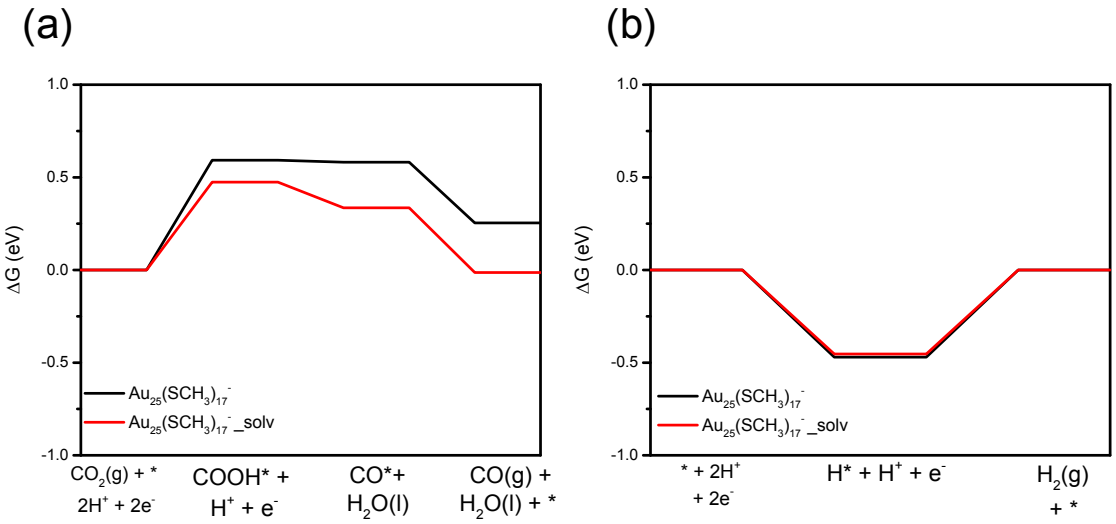

Figure S3. Free energy diagrams (ΔG) for the (a) reduction of CO_2 to CO and the (b) hydrogen evolution reaction on the $Au_{25}(SCH_3)_{17}^-$ NC with and without solvation effects in red and black, respectively. The $Au_{25}(SCH_3)_{17}^-$ NC and all reaction species were reoptimized with and without solvation in Turbomole using PBE/TZVP to utilize the implicit solvation model, COSMO.

-SCH_3 or -SEthPh removal

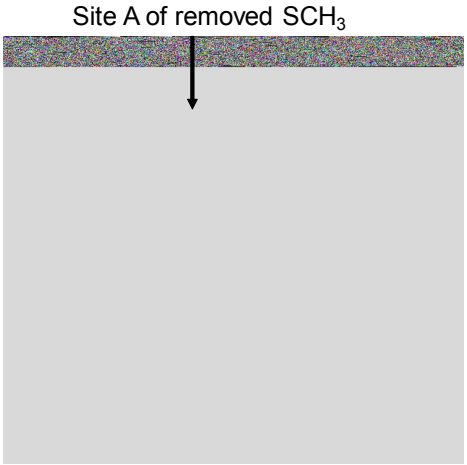

$\Delta E(Au_{25}(SCH_3)_{17}^{-})$: 1.14

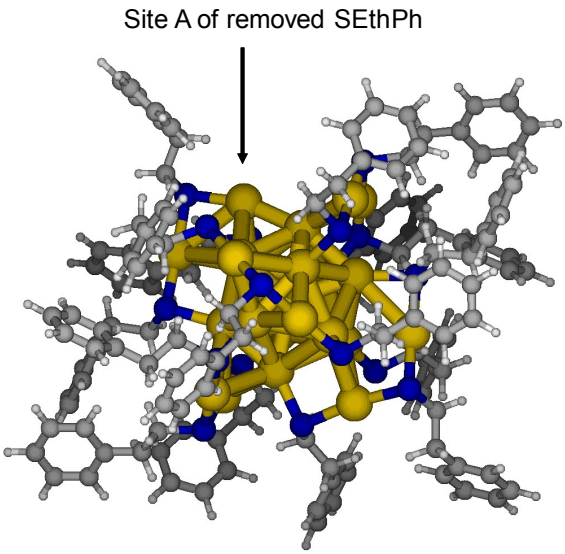

$\Delta E(Au_{25}(SEthPh)_{17}^{-})$: 1.31

-CH_3 or -EthPh removal

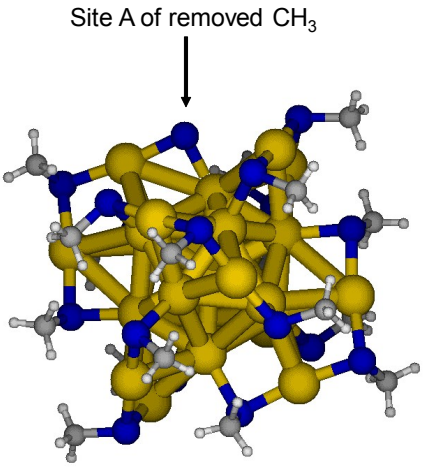

$\Delta E(Au_{25}S(SCH_3)_{17}^{-})$: -0.023

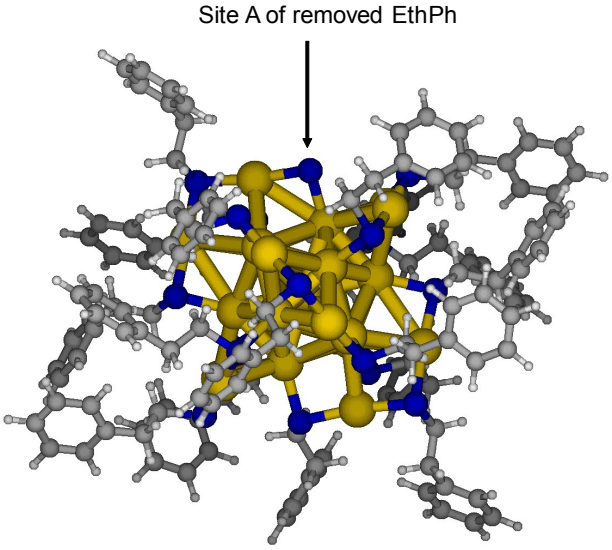

$\Delta E(Au_{25}S(SEthPh)_{17}^{-})$: 0.26

Figure S4. Electronic energy comparison for the reaction step of -SR and -R removal from $Au_{25}(SCH_3)_{18}^{-}$ and $Au_{25}(EthPh)_{18}^{-}$. The similar magnitude of the electronic energies between ligand removal on $Au_{25}(SCH_3)_{18}^{-}$ and $Au_{25}(SEthPh)_{18}^{-}$ suggests that similar trends would hold for free energies, as electronic energies capture the majority of enthalpic contributions. This indicates that under reaction conditions removal of experimentally utilized ligands (-SEthPh) is possible.

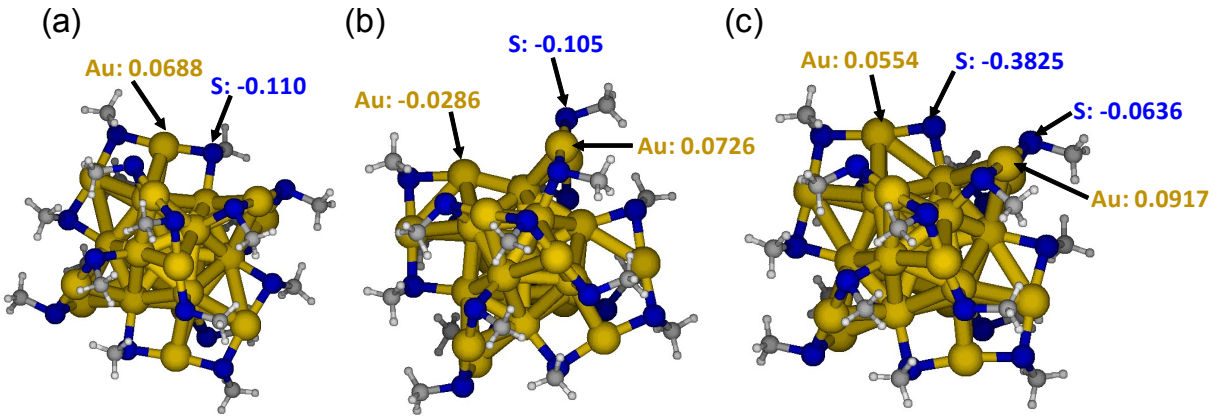

Figure S5. Bader charge analysis of select atoms from the negatively charged nanoclusters (a) $Au_{25}(SCH_3)_{18}^-$, (b) $Au_{25}(SCH_3)_{17}^-$, (c) $Au_{25}S(SCH_3)_{17}^-$.

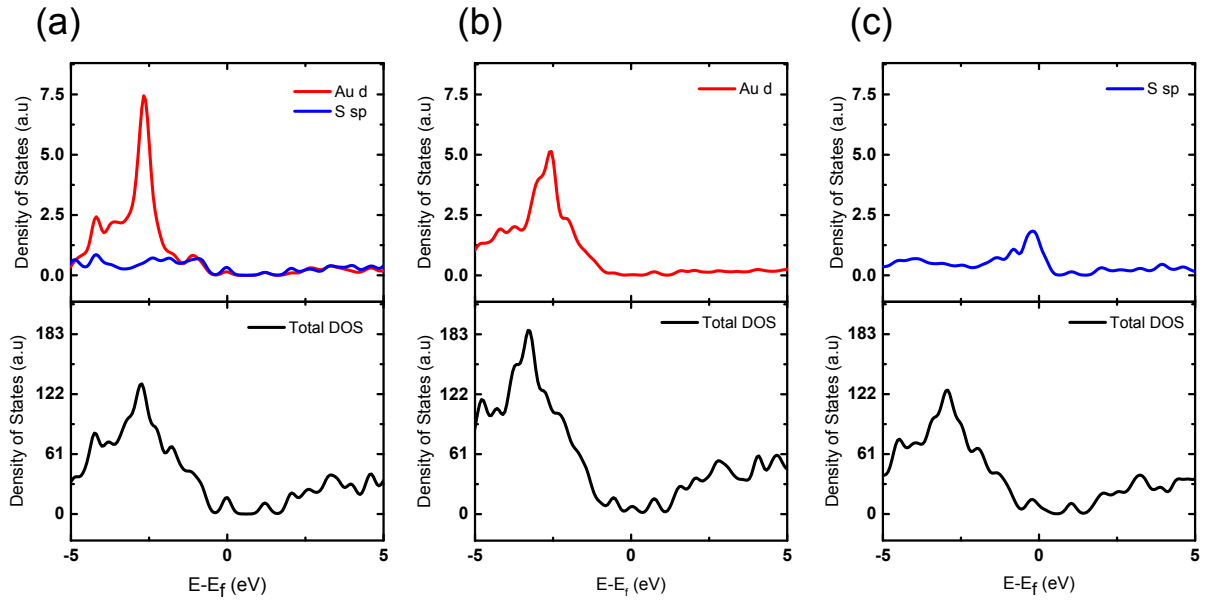

Figure S6: The projected density of states, PDOS (top graphs) for a ligand Au atom and a S atom of (a) $Au_{25}(SCH_3)_{18}^-$, the exposed Au atom of (b) $Au_{25}(SCH_3)_{17}^-$, and the exposed S atom of (c) $Au_{25}S(SCH_3)_{17}^-$. Comparison of the exposed S atom PDOS (s and p states) to the S atom PDOS of the fully protected NC, shows an increase in the electron density near the Fermi level (0 eV) of the $Au_{25}S(SCH_3)_{17}^-$ NC which contributes to the reactivity of the NC. The total density of states for the (a) $Au_{25}(SCH_3)_{18}^-$, (b) $Au_{25}(SCH_3)_{17}^-$, and (c) $Au_{25}S(SCH_3)_{17}^-$. NCs are shown in the bottom graphs.

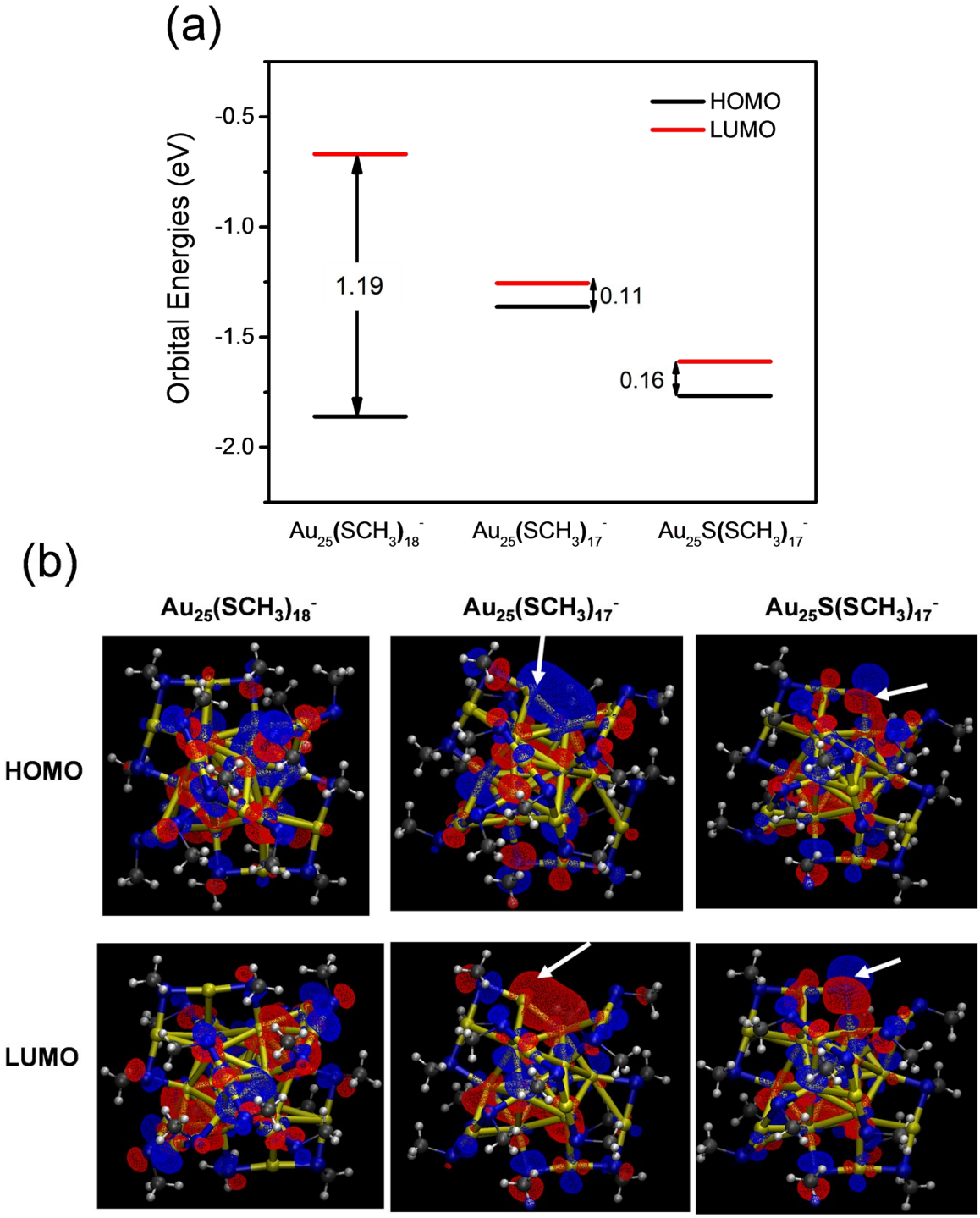

Figure S7. (a) HOMO-LUMO energy gaps (in eV) of the fully-protected and partially ligand-removed NCs. A dramatic decrease in the gap is observed with ligand removal. (b) Plots of the HOMO-LUMO orbitals. The white arrows point to the ligand removed sites ($-SCH_3$ and $-CH_3$) from the NCs. Compared to $Au_{25}(SCH_3)_{18}^-$, the electron density on the exposed Au site of $Au_{25}(SCH_3)_{17}^-$ becomes more localized and the exposed S site of $Au_{25}S(SCH_3)_{17}^-$ becomes more directional, both of which contribute to the reactivity of these generated sites.